A COMPUTATIONAL AEROELASTIC APPROACH TO PREDICT GALLOPING OF ICED CONDUCTORS WITH THREE DEGREES OF FREEDOM

Amir Borna*, Wagdi G. Habashi, Siva K. Nadarajah
Computational Fluid Dynamics Laboratory, Department of Mechanical Engineering, McGill University, Montreal, CANADA
*Corresponding Author: amir.borna@mail.mcgill.ca

Ghyslaine McClure
Department of Civil Engineering and Applied Mechanics, McGill University, Montreal, CANADA

***Abstract**:* Large oscillations of an elastically mounted iced cylinder in a uniform incident wind flow are studied with a three-degree-of-freedom model (with horizontal, vertical and torsional motions), using two-dimensional fluid-structure interaction (FSI) analysis. A Computational Fluid Dynamics (CFD) approach is adopted in the analysis, based on the Unsteady Reynolds-Averaged Navier-Stokes (URANS) equations and the Spalart-Allmaras one-equation turbulence model. These algorithms are implemented in a finite element code, yielding the time history of the detailed flow field around and in the wake of the iced cylinder. Vortex shedding from the iced cylinder is numerically investigated for moderate Reynolds numbers, and a Computational Structural Dynamics (CSD) module is used to determine the dynamic response of the cylinder based on the fluid flow loading and structural support characteristics.

1. INTRODUCTION

Wind-induced motions of iced conductors are of great interest. In particular, predicting conductor galloping has been a difficult task ever since overhead lines have been erected at the beginning of the last century. The majority of current predictive methods rely on field tests conducted on experimental line sections, wind tunnel experiments, or quasi-steady computations in which the aerodynamic lift and drag coefficients needed to compute the loading over conductors are obtained in wind tunnel tests [1]. Experimental set-ups are expensive and have difficulty replicating icing conditions at full scale, while quasi-steady computations require assumptions that compromise their applicability in the case of bundled leeward cables placed in the wake of other cables. In this work, in-plane cross-sectional oscillations of an elastically mounted iced-conductor are studied with a three-degree-of-freedom model in the horizontal, vertical and torsional directions using two-dimensional fluid-structure interaction (FSI) analysis. A CFD approach based URANS equations, using the Spalart-Allmaras turbulence model, is implemented via the finite element code, FENSAP-ICE [2].

2. RESULTS AND DISCUSSION

The maximum iced conductor displacements and fundamental frequencies of the motion in vertical, horizontal and torsional directions, vortex shedding, and galloping ellipses are plotted and discussed for different Reynolds numbers. In Figs. 1-2, typical results for vertical displacement, loading, and flow field are presented.

3. CONCLUSION

In this study, as a proof of concept, a numerical framework for studying cable-galloping instabilities as a fluid-structure interaction event is presented, and the results are validated against experimental results obtained by others and with several test cases. This framework can be used to numerically study iced conductors with arbitrary structural parameters and free stream conditions. Such a computational framework will, hopefully, provide a more detailed simulation tool to better understand the physics of cable galloping events and their effective mitigation.

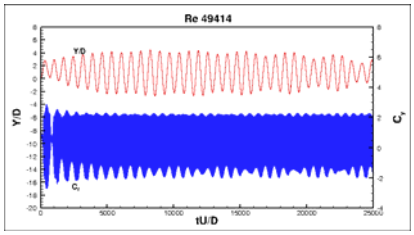

Figure 1: Vertical displacement and force coefficient versus non-dimensional time, Re 49414

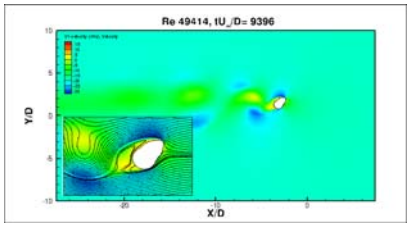

Figure 2: Flow field details and velocity magnitude contour at $tU_\infty/$ =9396, Re 49414

4. REFERENCES

[1] EPRI Transmission line reference book: Wind-induced conductor motion. 2006, EPRI, Palo Alto, CA: 2006. 1012317.

[2] Habashi W. G. , Aubé M., Baruzzi G., Morency F., Tran P., and Narramore J. C., FENSAP-ICE: A full-3d in-flight icing simulation system for aircraft, rotorcraft and UAVS, in 24th Congress of International Council of the Aeronautical Sciences. 2004: Yokohama, Japan

[3] J.-L. Lilien, P. Van Dyke, J.-M. Asselin, M. Farzaneh, K. Halsan, D. Havard, D. Hearnshaw, A. Laneville, M. Mito, C. B. Rawlins, M. St-Louis, D. Sunkle, and A. Vinogradov, State of the art of conductor galloping. Task force B2.11.06. 2007, CIGRE.

A Computational Aeroelastic Approach to Predict Galloping of Iced Conductors with 3 Degrees of Freedom

Amir Borna, Wagdi G. Habashi, Siva K. Nadarajah
Computational Fluid Dynamics Laboratory
Department of Mechanical Engineering
McGill University
Montreal, Canada

Ghyslaine McClure
Department of Civil Engineering and Applied Mechanics
McGill University
Montreal, Canada

***Abstract*— Large oscillations of an elastically mounted iced cylinder in a uniform incident wind flow are studied with a three- degree-of-freedom model (with horizontal, vertical and torsional motions), using two-dimensional fluid-structure interaction (FSI) analysis. A Computational Fluid Dynamics (CFD) approach is adopted in the analysis, based on the Unsteady Reynolds-Averaged Navier-Stokes (URANS) equations and the Spalart-Allmaras one-equation turbulence model. These algorithms are implemented in a finite element code, yielding the time history of the detailed flow field around and in the wake of the iced cylinder. Vortex shedding from the iced cylinder is numerically investigated for moderate Reynolds numbers, and a Computational Structural Dynamics (CSD) module is used to determine the dynamic response of the cylinder based on the fluid flow loading and structural support characteristics.**

Keywords- Aeroelasticity, Fluid-Structure interaction, Cable Galloping, Vortex Shedding, Iced Conductors

I. INTRODUCTION

Wind-induced motions of iced conductors are of great interest. In particular, predicting conductor galloping has been a difficult task ever since overhead lines have been erected at the beginning of the last century [1]. The majority of current predictive methods rely on field tests conducted on experimental line sections, wind tunnel experiments, or quasi-steady computations in which the aerodynamic lift and drag coefficients needed to compute the loading over conductors are obtained in wind tunnel tests [2]. Experimental set-ups are expensive and have difficulty replicating icing conditions at full scale, while quasi-steady computations require assumptions that compromise their applicability in the case of bundled leeward cables placed in the wake of other cables [2-4]. In this work, in-plane cross-sectional oscillations of an elastically mounted iced-conductor are studied with a three-degree-of-freedom model in the horizontal, vertical and torsional directions using two-dimensional fluid-structure interaction (FSI) analysis. A CFD approach based URANS equations, using the Spalart-Allmaras turbulence model, is implemented via the finite element code, FENSAP-ICE [5].

II. GOVERNING EQUATIONS

A. Fluid Dynamics

In this study, the URANS equations are solved using FENSAP-ICE, a second order accurate 3D finite element compressible Navier-Stokes solver [5-7]. The one-equation Spalart-Allmaras [8] turbulence model is applied to estimate the Reynolds stresses. To handle the moving nodes on the fluid/structure boundary and determine the new positions of internal nodes in the fluid domain, the Arbitrary Lagrangian Eulerian (ALE) formulation of Navier-Stokes equations is applied [9]. The non-dimensional URANS equations used in FENSAP-ICE can be expressed as follows.

$$\frac{\partial \rho}{\partial t} - \bar{u}_i \rho_{,i} + \left(\rho u_i\right)_{,i} = 0 \tag{1}$$

$$\frac{\partial \rho u_i}{\partial t} - \bar{u}_i \left(\rho u_i\right)_{,i} + \left(\rho u_i u_j\right)_{,j} = -p_{,i} + \mathrm{Re}_\infty^{-1} \tau_{ij,j} - \left(\rho \overline{u_i u_j}\right)_{,j} \tag{2}$$

where ρ is density, t time, u_i the i^{th} component of velocity, $\bar{u}_i$ mesh velocity, p pressure, τ stress tensor, Re_∞ free stream Reynolds number, and $\rho\overline{u_i u_j}$ the Reynolds stress tensor.

B. Rigid Body Dynamics

In the FSI analysis, the iced conductor is treated as a rigid body mounted on flexible supports. In small kinematics, its cross-sectional motion along three degrees-of-freedom in vertical, horizontal, and torsional directions can be described by the following linear system of equations assuming viscous damping:

$$[M]\{\ddot{q}\} + [C]\{\dot{q}\} + [K]\{q\} = \{F\} \tag{3}$$

where $\{q\} = (x, y, \theta)^T$ is the displacement vector, [M] the mass/inertia matrix, [C] the structural viscous damping matrix, [K] the stiffness matrix, and {F} the fluid loading vector resulting from fluid surface loads. Note that [C] and [K] represent the characteristics of the supports only.

C. Coupling Algorithm

A general coupling algorithm with capability of handling conductors in 3D is designed in view of future full 3D studies. This algorithm includes three main modules (Fig. 1): the fluid solver, the solid solver, and the load/motion transfer operator that relays relevant analysis parameters between the two solution domains. Coupling starts with an initial flow field solution that provides the surface fluid tractions along the fluid mesh interface with the solid. Then, through the conservative load transfer module [10], surface tractions are integrated to yield the resultant nodal forces and moments applied on the solid mesh interface. The solution of Eq. (3) provides the cross-sectional conductor displacements, velocities and accelerations at every time step. In this study the direct integration operator used by the solid solver is the unconditionally stable Beta Newmark algorithm [11-13]. After each time increment, the solid displacements are imposed by compatibility to the nodes of the fluid mesh defined along the interface of the fluid domain with the solid, using the motion transfer module [10]. Then, the fluid solver handles this interface motion and computes the fluid mesh motion in the entire domain and solves the flow field. This loop marches in time until the total analysis duration is achieved.

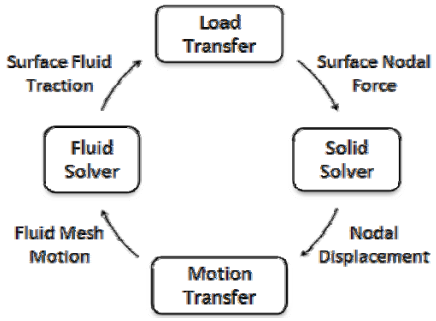

Figure 1: Global coupling and FSI (fluid-structure interaction) framework

As a starting point for the computations, the initial flow solution around the body is required; however, at the first time step, there is no converged CFD solution available yet. One common approach in the literature for fluid-structure interaction problems to circumvent this problem of implicit initial conditions is to let the flow around the body establish completely until shedding vortices reach their unsteady limit cycle. From that point forth, the body starts to move freely [14]. In this study, initialization has been done differently. First, a few time iterations have been performed in order to get a time-accurate flow established around the conductor without reaching to the limit cycle, and then the conductor is freed to move. Since the source of vortex shedding behind the bluff body is flow instabilities, this method helps to reach the limit cycle sooner and models the physical problem more accurately. Therefore, in all test cases, the conductor starts to move from rest, i.e.

$$\{q\}_{t=0} = \{q_0\} \text{ and } \{\dot{q}\}_{t=0} = \{0\}. \quad (4)$$

III. Model and Parameters

Fig. 2 illustrates the geometry of the model and the flow boundary conditions. The predefined ice profile is M. Tunstall's shape #1 [15], with maximum thickness of 132% of the bare cable radius, adapted over a conductor cross section with 32.5-mm diameter. The initial angle of attack of the incident wind on the iced conductor is 30 degrees, which also corresponds to the initial ice accretion angle in this problem. The non-dimensional time step, $U_\infty \Delta t/d$, is selected as 0.05 for all Reynolds numbers, on the basis of satisfactory numerical performance. In Fig. 2, the fluid mesh shown is defined by 30,000 nodes and the fluid domain dimensions are established according to the parameter D, the diameter of the bare conductor. The fluid mesh is structured as an O-grid around the body and an H-grid elsewhere. The closest nodes to the body are placed within $y^+<1$, and the next few nodes are placed within $y^+<5$, at all times and Reynolds numbers.

Structural properties are taken from [16]. The natural frequencies (in Hz) of the solid bluff body on flexible supports are 0.995, 0.845, and 0.865 in the horizontal, vertical, and torsional directions, respectively. The mass per unit length is 3.25 kg/m, and based on available data and geometry, the mass moment of inertia per unit length is estimated as 0.0394 kg-m^2/m (there is no explicit value for this parameter in [16]). The structural damping is set to 0.08% of critical viscous damping for horizontal and vertical motion, and 0.3% for rotation.

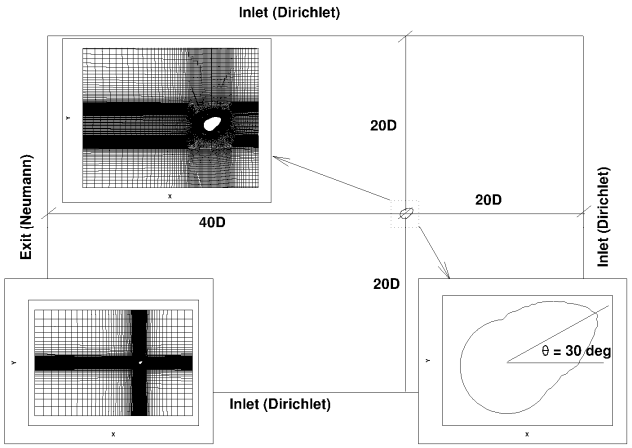

Figure 2: Model Dimensions, mesh (O-H), and Boundary Conditions

IV. Results and Discussion

A. Validation

The FENSAP flow solver has been extensively validated with different test cases [17]. In addition, results of the current computational framework have been validated for vortex-induced vibration of cylinders. Finally, for this study, the computational results are compared in Table 1 with those available from wind tunnel experiments reported in [18]. There is agreement between the numerical and wind tunnel results: The frequency is the same for the three directions of motion in each case, with a 3% underestimation from the computational model. There is more variability in the prediction of the amplitude of the translational oscillations, with a maximum difference of about 8%. However, torsional amplitudes are different. As

the response frequencies and other amplitudes are in good agreement, this large difference can probably be attributed to the value of the mass moment of inertia used in the model, which could only be estimated from the available data in [16].

Table 1: Comparison of results with [18]

Test	U(m/s)	Re	Amplitude			f_0 (Hz)		
			A_X/D	A_Y/D	θ°	X	Y	θ
Current	9.7	24707	0.55	0.85	5.6	0.85	0.86	0.86
Ref. [18]	9.7	24707	0.51	0.91	15.2	0.89	0.89	0.89

f_0 is the frequency of the motion of the solid body, **A** max amplitude, **X** horizontal, **Y** vertical, and **θ** rotational.

B. Results

The main results discussed here are the maximum response in displacements of the iced conductor shape and the fundamental (lowest) frequencies of its motion in the vertical, horizontal and torsional directions for different Reynolds numbers. The incident flow conditions vary from wind speeds of 2.4 to 19.4 m/s, corresponding to Re values of 6000 to over 49400. Clearly, as expected, the iced conductor response motion is completely different than that of the cylindrical bare conductor.

Table 2 summarizes the results obtained from the numerical simulations. It is seen that in the range of Reynolds numbers studied, the fundamental frequencies of the cable motion (f_0) are close to the natural frequencies of the oscillator (f_n), i.e. the frequency ratio, f*, is close to unity (see Table 2). However, this is not the case for the horizontal motion (X-direction) with Re of 18000 and 24700, where the frequency ratio drops under 0.88, indicating that the forced motion has a longer period of oscillation. We are investigating whether these results have a physical basis or not.

Except for these two Re cases, the amplitudes of conductor motion tend to increase monotonically with Reynolds number. The case of Re 18000 was found to be particular, while the results obtained for Re 24707 compare well with the other values of Re in terms of general trends in time history response, flow field and trajectory illustrated in Figs. 4 to 13.

Table 2: Amplitudes and fundamental frequencies of conductor motion

Re	Amplitude			f_0 (Hz)			$f^*=f_0/f_n$		
	A_X/D	A_Y/D	θ°	X	Y	θ	X	Y	θ
6000	0.043	0.048	0.38	0.992	0.839	0.870	0.997	0.993	1.006
9000	0.084	0.105	0.84	1.000	0.848	0.865	1.005	1.004	1.000
12736	0.143	0.215	1.56	0.977	0.854	0.854	0.982	1.011	0.987
18000	0.288	1.806	7.54	0.875	0.849	0.875	0.879	1.005	1.012
24707	0.552	0.849	5.62	0.839	0.858	0.858	0.843	1.015	0.992
49414	3.903	3.577	23.52	0.992	0.824	0.810	0.997	0.975	0.936

In Table 3, the dominant (fundamental) frequencies of the equivalent loads are summarized. Unlike the conductor motion, this dominant frequency is the same in all three directions, since these loads are obtained from the fluid surface tractions. These frequencies are much higher (more than 10 to 70 times) than the resulting dominant frequency of the cable motion. Several time history results show beating phenomena, where high-frequency loading fluctuations are combined to lower frequency conductor motions (see Figs. 4 to 6 with 8 to 10). Finally, as expected, the dominant loading frequencies increase with Reynolds number and vary almost linearly with incident wind speed.

Table 3: Fundamental frequencies of conductor loading

Test #	U(m/s)	Re	f_0 (Hz)		
			X	Y	θ
1	2.4	6000	10	10	10
2	3.5	9000	15	15	15
3	5.0	12736	20	20	20
4	7.1	18000	25	25	25
5	9.7	24707	40	40	41
6	19.4	49414	68	68	64

In the following sections, detailed results for two Reynolds numbers, 9000 and 49414, are presented. Only the galloping ellipses are presented for the other test cases.

1) Reynolds 9000

Fig. 3 shows the detailed flow field and stream lines around the body at non-dimensional time (tU_∞/d) of 6108 for Re 9000. The flow is separated in a large part of the body and the location of the separation points oscillates because of the inherent flow instabilities behind the body. Alternating separation points develop an unsteady vortex street in the back of the body. Also, the pressure distribution around the body changes due to this instability in separation. This creates time-variant loading over the body that is sometimes large enough to induce noticeable displacements, known as vortex-induced vibrations.

Figs. 4 to 6 show the time history of displacements and loading for the three degrees-of-freedom, X, Y and θ, respectively. It is seen from these figures that, although the loading is sustained (amplitude and frequency in all directions do not decrease in time), the horizontal and torsional motion amplitudes decrease with time, while only the vertical amplitude is sustained. As the structural damping included in the model is very small (0.08% viscous critical in each direction), the amplitude decay in the horizontal and torsional directions is mainly attributed to positive aerodynamic damping. Clearly, this effect is not as large in the vertical direction as seen in Fig. 5.

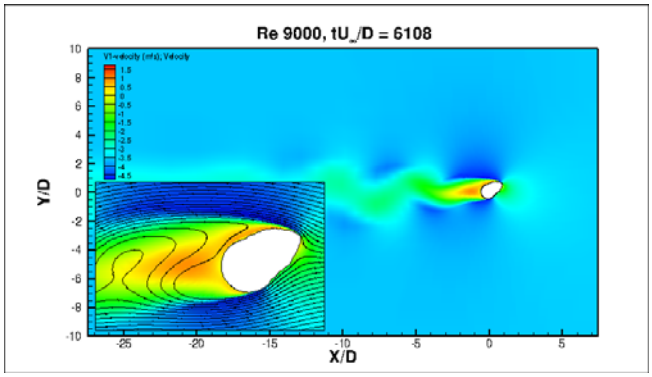

Figure 3: Flow field details and velocity magnitude contour at tU_∞/d=6108, Re 9000

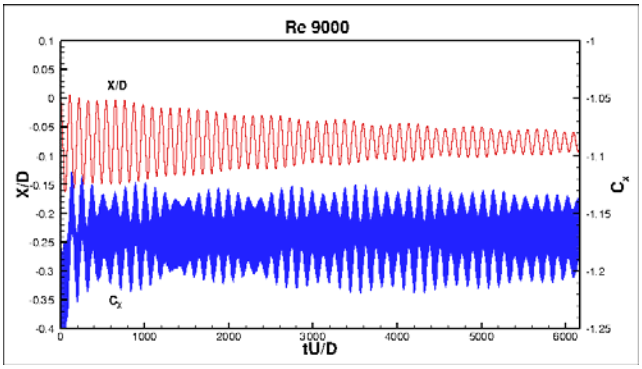

Figure 4: Horizontal displacement and force coefficient versus non-dimensional time, Re 9000

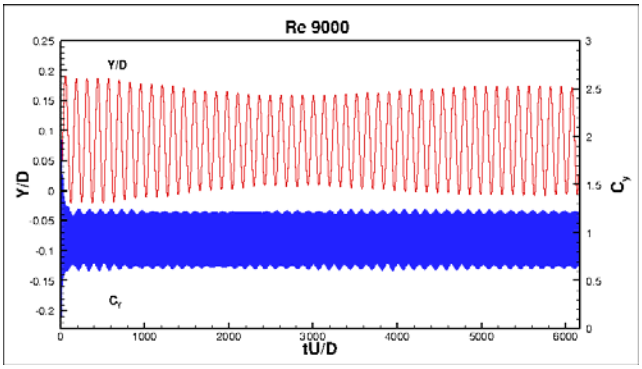

Figure 5: Vertical displacement and force coefficient versus non-dimensional time, Re 9000

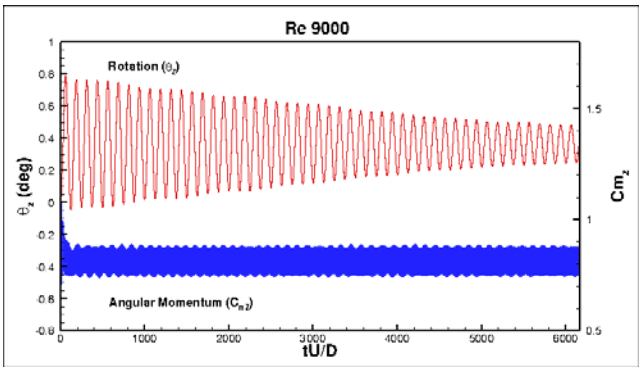

Figure 6: Rotation and angular momentum coefficient versus non-dimensional time, Re 9000

2) Reynolds 49414

The vortex street, structural response, and unsteady loading in Re 49414 are different than in the other test cases. Fig. 7 shows the flow field and streamlines around the body at tU_∞/d = 9396. The frequency of vortex shedding in this case is higher.

Figs. 8 to 10 show plots of displacements and loading versus non-dimensional time. After vortex shedding has developed, the amplitude of the horizontal displacement increases with time and a regular beating pattern is observed in Fig. 8. This beating is also present in the torsional response (Fig. 10), but the maximum amplitude of the rotational motion does not increase, and reaches a non-variant value. Unlike these two directions, the vertical motion response (Fig. 9) does not show any beating and the maximum amplitude remains almost the same through time.

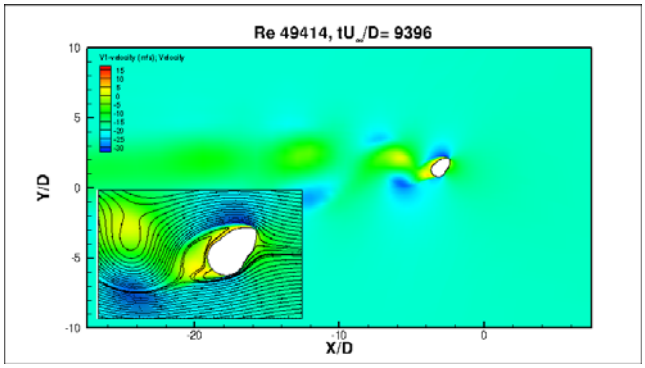

Figure 7: Flow field details and velocity magnitude contour at $tU_\infty/$ =9396, Re 49414

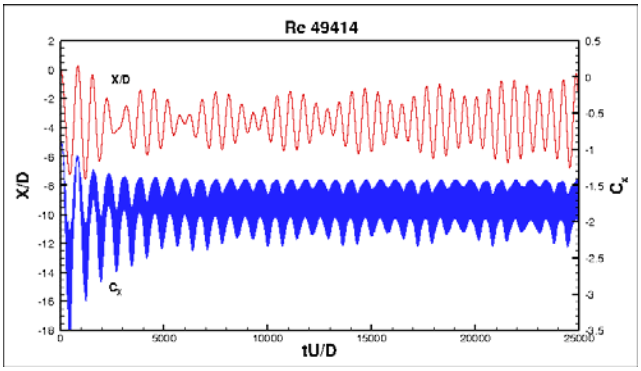

Figure 8: Horizontal displacement and force coefficient versus non-dimensional time, Re 49414

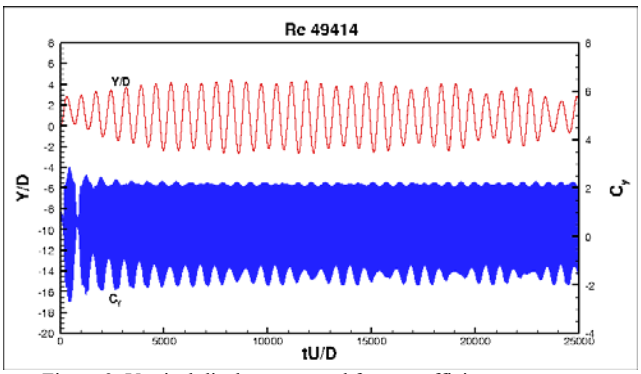

Figure 9: Vertical displacement and force coefficient versus non-dimensional time, Re 49414

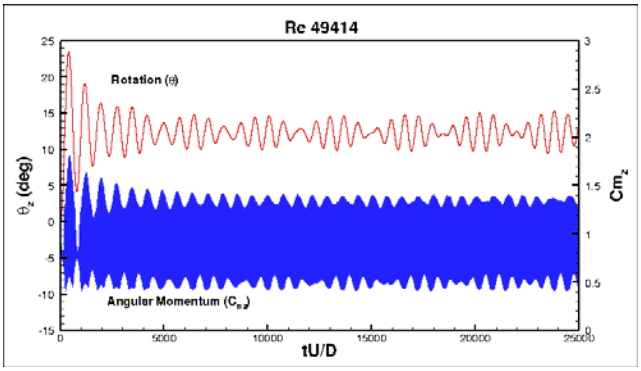

Figure 10: Rotation and angular momentum coefficient versus non-dimensional time, Re 49414

3) Galloping Ellipses

The trajectory of the centroid of the iced conductor in the x-y plane is referred to as the galloping ellipse. The size and shape of this trajectory are important in transmission line design. Therefore, in this section, galloping ellipses are presented for all six test cases.

Fig. 11 shows the galloping ellipses for Re 6000 and 9000. At these Reynolds numbers, initially, the conductor motion starts with similar amplitudes in both the horizontal and vertical directions, making for an X-shaped trajectory. Then, after a sustained motion is established, the horizontal amplitude decreases, while the vertical amplitude is almost invariant, and the ellipses become narrower in the horizontal direction (see denser lines in the figure).

For higher Reynolds numbers (see Figs. 12 and 13a), the ratio of vertical to horizontal amplitudes is larger than unity from the start, and the galloping ellipses become progressively more vertical. However, these motion trends are lost when increasing Reynolds number beyond 49000 (Se Fig. 13b) and the elliptic trajectories appear random.

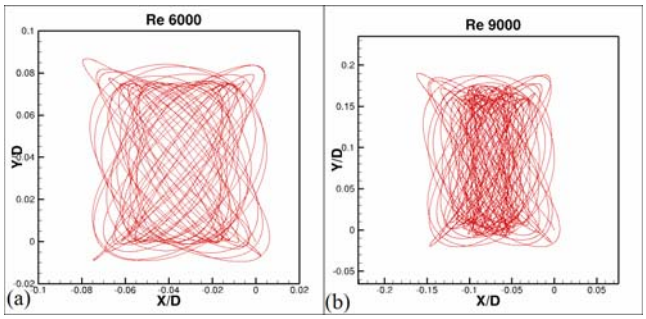

Figure 11: X-Y trajectory, (a) Re 6000, (b) Re 9000

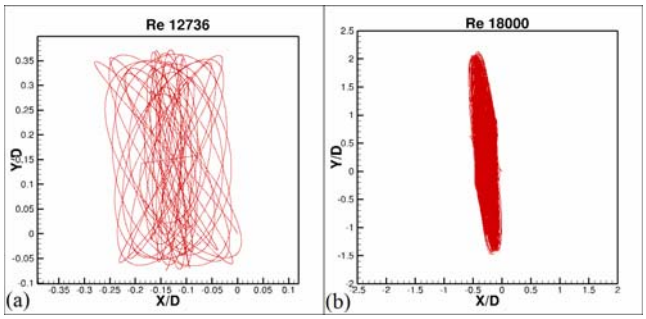

Figure 12: X-Y trajectory, Re 12736 (a), Re 18000 (b)

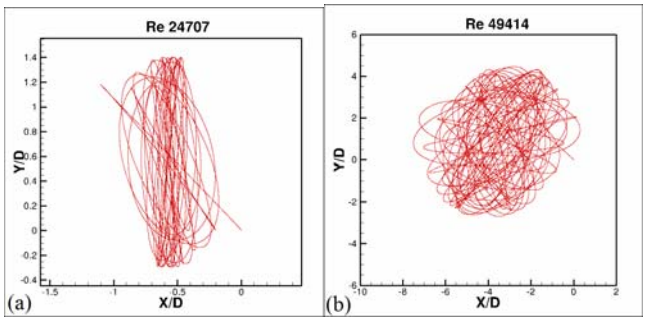

Figure 13: X-Y trajectory, Re 24707 (a), Re 49414 (b)

I. CONCLUDING REMARKS

In this study, as a proof of concept, a numerical framework for studying cable-galloping instabilities as a fluid-structure interaction event is presented, and results are validated against experiments. This framework is general and can be used to study iced conductors with any specified structural parameters at any free stream conditions. Such a computational framework will eventually provide a powerful simulation tool that will permit a better understanding of the physics of cable galloping events and their effective mitigation.

ACKNOWLEDGMENTS

The authors would like to acknowledge funding from the Fonds québécois de la recherche sur la nature et les technologies (FQRNT) in the form of a research team grant.

REFERENCES

[1] C. H. K. Williamson and R. Govardhan, "Vortex-Induced Vibrations". Annual Review of Fluid Mechanics, 2004. 36(1): p. 413-455.

[2] EPRI Transmission line reference book: Wind-induced conductor motion. 2006, EPRI, Palo Alto, CA: 2006. 1012317.

[3] M. Farzaneh, ed. Atmospheric icing of power networks. 1 ed. 2008. 381.

[4] J.-L. Lilien, P. Van Dyke, J.-M. Asselin, M. Farzaneh, K. Halsan, D. Havard, D. Hearnshaw, A. Laneville, M. Mito, C. B. Rawlins, M. St-Louis, D. Sunkle, and A. Vinogradov, State of the art of conductor galloping. Task force B2.11.06. 2007, CIGRE.

[5] Habashi W. G. , Aubé M., Baruzzi G., Morency F., Tran P., and Narramore J. C., FENSAP-ICE: A full-3d in-flight icing simulation system for aircraft, rotorcraft and UAVS, in 24th Congress of International Council of the Aeronautical Sciences. 2004: Yokohama, Japan

[6] O. C. Zienkiewicz, R. L. Taylor, and J. Z. Zhu, The finite element method : its basis and fundamentals. 2005, Oxford ; Boston :: Elsevier Butterworth-Heinemann.

[7] Habashi W. G., "Advances in CFD for In-Flight Icing Simulation". Journal of Japan Society of Fluid Mechanics, 2009. 28(2): p. 99-118.

[8] J. E. Bardina, Huang, P. G., Coakley, T. J., Turbulence modeling validation, testing, and development. NASA technical memorandum 110446. 1997, Moffett Field, Calif.: National Aeronautics and Space Administration, Ames Research Center ; National Technical Information Service.

[9] E. Stein, R. D. Borst, and T. J. R. Hughes, Encyclopedia of computational mechanics. 2004, Chichester, West Sussex :: John Wiley.

[10] C. Farhat, M. Lesoinne, and P. Le Tallec, "Load and motion transfer algorithms for fluid/structure interaction problems with non-matching discrete interfaces: Momentum and energy conservation, optimal discretization and application to aeroelasticity". Computer Methods in Applied Mechanics and Engineering, 1998. 157(1-2): p. 95-114.

[11] K.-J. Bathe, Finite Element Procedures. 2007: Klaus-Jurgen Bathe.

[12] W. Dettmer and D. Peric, "A computational framework for fluid-rigid body interaction: Finite element formulation and applications". Computer Methods in Applied Mechanics and Engineering, 2006. 195(13-16): p. 1633-1666.

[13] S. Rao, Mechanical Vibrations. 2004: Pearson Prentice Hall.

[14] E. Guilmineau and P. Queutey, "Numerical simulation of vortex-induced vibration of a circular cylinder with low mass-damping in a turbulent flow". Journal of Fluids and Structures, 2004. 19(4): p. 449-466.

[15] M. Tunstall and L. T. Koutselos, Further studies of the galloping instability & natural ice accretion on overhead line conductors, in 4th Int. Conf. on Atmospheric Icing of Structures. 1998: Paris.

[16] R. Keutgen and J. L. Lilien, "Benchmark cases for galloping with results obtained from wind tunnel facilities validation of a finite element model". Power Delivery, IEEE Transactions on, 2000. 15(1): p. 367-374.

[17] Newmerical Technologies Int., "NTI solutions, Manual and test cases for FENSAP-ICE". unpublished.

[18] O. Chabart and J. L. Lilien, "Galloping of electrical lines in wind tunnel facilities". Journal of Wind Engineering and Industrial Aerodynamics, 1998. 74-76: p. 967-976.